EFFECT OF GRAIN SIZE ON THE DRAWABILITY OF THE NIOBIUM-STABILIZED FERRITIC STAINLESS STEEL ASTM 430*

Caio César Caldeira Moura[1]
Reginaldo Pinto Barbosa[2]
Tarcísio Reis de Oliveira[3]

Abstract

Studies were carried out with samples of AISI 430 stainless steel stabilized with niobium produced by direct reduction (just one cold rolling process) in order to evaluate the grain size on material deep drawability. Recrystallized samples were heat treated in the laboratory promoting the growth of the recrystallized grain. Microstructural characterizations were done by X-ray diffraction for evaluating crystallographic texture, optical microscopy and electron backscatter diffraction (EBSD). The drawability was evaluated by tensile tests for the determination the planar (ΔR) and normal (r) anisotropy coefficients. The increase in grain size promoted an increase in the intensity of the Gamma fiber (beneficial) and reduction Theta fiber (damaging) on the surface of material thickness. At the center of thickness, it was observed that the Gamma fiber intensity did not change significantly, and the Theta fiber intensity was reduced. The change of the crystallographic texture, promoted by the increase of grain size, increased the coefficient of anisotropy (r) in all directions analyzed and decreased the planar anisotropy coefficient.

Keywords: Anisotropy; Texture; Grain Size; Deep Drawability.

[1] *Mechanical Engineering, Research & Development Intern, Aperam South America, Timóteo, Minas Gerais, Brazil.*
[2] *Master's degree in Mechanical Engineering, Researcher Senior, Research Center, Aperam South America, Timóteo, Minas Gerais, Brasil.*
[3] *Doctor's Degree in Science and Engineering Materials, Research Center Manager, Research Center, Aperam South America, Timóteo, Minas Gerais, Brazil.*

1 INTRODUCTION

Stainless steels have excellent corrosion resistance and elevated mechanical properties which allow them to be used in several applications in aggressive environments. In relation to the current stainless steel family, ferritic stainless steels are used in applications that require high corrosion resistance, good surface quality and good formability [1].

In the 90's, Aperam South America developed a ferritic stainless steel ASTM 430 stabilized with Niobium, aiming to improve the formability of this steel [1]. The addition of Niobium inhibits the material recrystallization during the hot rolling process through the precipitation of Niobium carbonitride and the effect of Niobium in solid solution, resulting in a hot rolled coil with more refined and homogeneous structure, improving the properties of the final product [2].

The performance of ferritic steels is different in relation to the austenitic ones as regards the formability. During stamping, austenitic steels have a good stretching resistance and good strain distribution, allowing the construction of pieces with more complex geometries. Ferritic stainless steels are used for stamping pieces where the deep drawing processes is predominant [3].

The ferritic stainless steel formability can be evaluated by the Lankford coefficient $r(\alpha)$, which is defined by the ratio of true strain in width and thickness of a specimen during a tensile test in relation to rolling direction according to an α angle. Materials with high average normal anisotropy value, $\bar{r}$, and low planar anisotropy value, ΔR, have a low reduction in their thickness and low strain variation in their plane during the deep drawing process. Features that are advantageous for deep drawing applications [4, 5].

In this paper, the influence of the recrystallized grain size increasing of the 430Nb stainless steel with 0.6 mm thickness was evaluated in the evolution of crystallographic texture, anisotropy and, consequently, their formability.

2 MATERIAL AND METHODS

The samples used in the study were taken out from a coil of a Niobium-stabilized ferritic stainless steel AISI 430 (430Nb) annealed in an industrial continuous furnace with a heating rate of 24 °C.s^{-1} after a cold rolling process with 85% reduction in thickness. The samples chemical composition is shown in Table 1.

Table 1. Chemical composition of the 430Nb samples.

C	Mn	Si	Cr	N	Ni	Nb
0.018	0.202	0.36	16.2	0.032	0.31	0.24

Units in %mass.

Heat treatment: The samples were annealed in an industrial furnace according to Table 2. After that, the samples identified by BF-02, BF-03 and BF-04 were submitted to an additional annealing process on a stationary furnace. This second annealing process had the objective to increase the material recrystallized grain size.

Table 2. Heat treatment of samples.

Samples	IT (°C)	AT (°C)	t (s)
BF-01	885 ± 15	-	15 ± 1,5
BF-02	885 ± 15	915 ± 1	15 ± 1,5
BF-03	885 ± 15	965 ± 1	15 ± 1,5
BF-04	885 ± 15	1015 ± 1	15 ± 1,5

IT – Industrial heat treatment
AT– Additional heat treatment
t – Soaking time
GS – Grain Size in ASTM

Microstructure Analysis: The samples were prepared through standard metallographic procedures (cutting, mounting, grinding and mechanical polishing) and analyzed through their longitudinal sections after etching with Villela reagent for 50s. The average grain size was measured using the Abrams Concentric Circles method according to ASTM E111-13 [6].

Texture Analysis: The crystallographic orientation intensity in the surface and center of the samples were analyzed using the X-ray diffraction method with the aid of X'Pert Philips® equipment and the software OIM Analysis®. This information allowed to get the orientation distribution functions ODFs (Euller angles according to Bunge propose) in φ_2 = 45°.

The industrial coil textures were collected through the Eletron Backscatter Diffraction (EBSD) method, using the software EDAX® on FEI-Quanta 250 FEG® electron microscope. Then, the orientation distribution functions (ODFs) and volumetric fractions were analyzed by OIM Analysis software®.

Mechanical Properties: Tensile tests were carried out, at room temperature, on INSTRON 5583 equipment according to ASTM E8/E8M standard [7]. The average normal anisotropy value, $\bar{r}$, was calculated using equation 1.

$$\frac{r_0+2r_{45}+r_{90}}{4} \quad (1)$$

Where r_0, r_{45} and r_{90} correspond to the $r(\alpha)$ values in the 0°, 45°, 90° directions in relation to rolling direction of the sheet metal, respectively. The planar anisotropy value, ΔR, was calculated according to equation 2 [9].

$$\frac{r_0-2r_{45}+r_{90}}{2} \quad (2)$$

3 RESULTS AND DISCUSSION

3.1 Microstructure

Figure 1 (a) shows the microstructure of a 430Nb 0.60 mm-thick coil annealed in an industrial continuous furnace. The samples microstructure with an additional heat treatment on a stationary furnace are shown in figures 1(b), (c), and (d). The additional heat treatment process promoted an increase of the average grain size through the migration of the previous grain boundaries in the recrystallized structure [8].

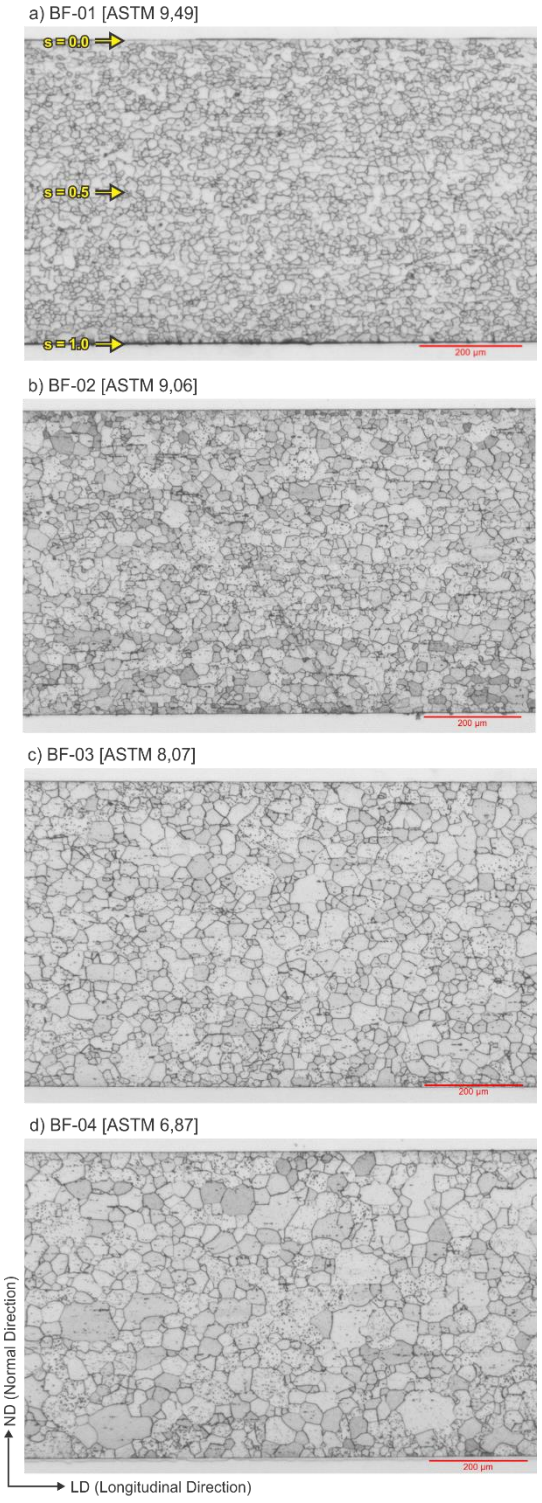

Figure 1. Microstructure of 430Nb samples after the heat treatment. (a) No additional heat treatment, (b) with additional heat treatment of 915ºC, (c) with additional heat treatment of 965ºC and (d) with additional heat treatment of 1015ºC ($\boldsymbol{s = 0}$ for surface layer and $\boldsymbol{s = 0,5}$ for center layer).

BF-01 and BF-02 samples presented a homogeneous recrystallized ferritic structure along their thickness, precipitates distributed throughout the matrix and ASTM 9.49 and ASTM 9.065 grain size, respectively. BF-03 and BF-04 samples presented heterogeneity on structure along their thickness, precipitates distributed throughout the ferritic matrix and ASTM 8.07 and ASTM 6.87 grain size, respectively.

3.2 Mechanical Properties

The sheet formability can be evaluated through the average normal anisotropy value, $\bar{r}$, and low planar anisotropy value, ΔR [5,9]. The average normal anisotropy indicates the sheet ability to resist thickness thinning when subjected to the tensile or compressive stress. The planar anisotropy indicates the strain variation in the sheet plane during the deformation. Materials with high values of average normal anisotropy and low values of planar anisotropy have a better performance in deep drawing process [4].

During the stamping process, the sheet strain occurs in all directions (0º to 360º) on sheet plan. Therefore, the rupture will occur, in this case, in the direction with less thinning resistance. Thus, the analyze of the formability considers the r for all directions [1].

Table 3 shows that the increase in grain size promoted the increase of r in all directions until ASTM 8,07 grain size (BF-03). The sample BF-04 had a reduction in r in all directions, when compared to sample BF-03. The ΔR was reduced with the increase of the average grain size.

The total elongation followed the same trend as the average normal anisotropy, increasing from 31.5% to 33.7% with grain size increasing from ASTM 9.49 (BF-01) to ASTM 8.07 (BF-03). While the sample BF-04, with a grain size ASTM 6.87, presented reduction in their total elongation to 33.5% when compared to sample BF-03.

Table 3. Mechanical properties of samples.

Samples	$r0°$	$r45°$	$r90°$	$\bar{r}$	ΔR	Te
BF01	1,59	1,10	1,96	1,44	0,68	31,5
BF02	1,64	1,33	2,31	1,65	0,65	32,5
BF03	1,80	1,70	2,73	1,98	0,57	33,7
BF04	1,42	1,66	2,23	1,74	0,16	33,5

Te – Total Elongation [%];

3.3 Texture

Orientation Distribution Functions (ODFs) on Bunge notation (figure 2) of samples are shown in Figure 3, where the coefficient “s” informs the analysis position along the thickness (figure 1). In general, the samples had a recrystallization texture in the $(334)[4\bar{8}3]$ component which is typical of a cold rolled ferritic stainless steel with direct rolling process [5,9]. This texture can be explained by the preferential growth of the component $(334)[4\bar{8}3]$ around the rolled component $(112)[1\bar{1}0]$ of the α fiber, due to the oriented growth mechanism caused by the selective drag of segregated particles in the grain boundaries [9, 10]. The other higher intensity was found at $(111)[\overline{11}2]$.

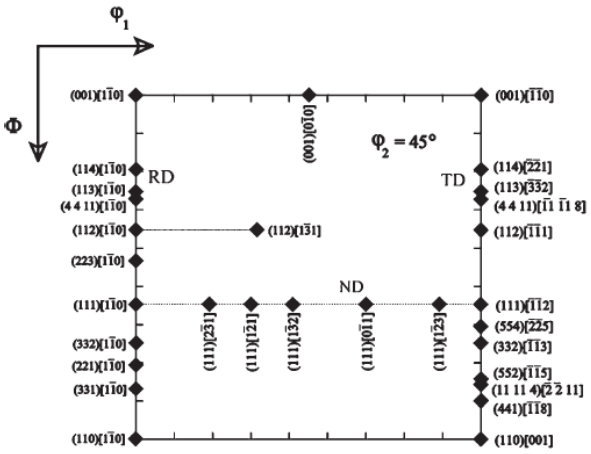

Figure 2. Section for φ_2 = 45º showing the position of main orientations along with the RD, TD and ND. Euler angles on notations proposed by Bunge [12].

On the surface of the thickness (s = 0), the increase of the average grain size reduced the intensity of the Theta fiber $(100)[uvw]$ (table 4). The intensities of the $(111)[1\bar{2}1]$

and $(111)[\bar{1}\bar{1}2]$ components of the γ fiber increased with the average grain size growth until ASTM 8.07 (BF03-S). At the center of the thickness (s = 0.5), the γ fiber showed the highest intensity for the ASTM 8.07 (BF03-C) average grain size and the intensity of the Theta fiber $(100)[uvw]$ was reduced with increased average grain size (Table 5).

Table 4. Volumetric fractions [%] and Gamma/Theta ratios of surface samples.

Sample	Rotated Cube (001)[110]	Theta (100)[uvw]	Gamma (111)//ND	Gamma/Theta
BF01-S	2,82	9,29	40,28	4,36
BF02-S	2,60	9,09	41,42	4,56
BF03-S	1,66	7,43	43,31	5,83
BF04-S	1,38	7,63	41,66	5,46

ND – Normal Direction.

The increase of the average normal anisotropy coefficient, i.e, the ability to withstand thinning, is strongly related to the increasing Gamma fiber components and the reduction of Theta fiber components [4, 9, 11]. The increase of the Theta fiber reduces the material formability due to the low r of the crystallographic orientations present in this fiber, especially in $r45°$ [5].

Table 5. Volumetric fractions [%] and Gamma/Theta ratios of center samples.

Sample	Rotated Cube (001)[110]	Theta (100)[uvw]	Gamma (111)//ND	Gamma/ Theta
BF01-C	2,83	9,56	40,11	4,20
BF02-C	2,90	10,09	39,40	4,90
BF03-C	2,10	8,76	40,42	4,62
BF04-C	1,40	8,27	39,68	3,80

ND – Normal Direction.

It is interesting to note that the values of r (table 3) showed a good correlation with the Gamma/Theta ratio values (tables 4 and 5), in which the sample BF-03 had, at surface (s = 0) and center (s = 0,5), the highest values. The optimum r point (BF-03) occurred due to growth of random components, displaced from the γ fiber axis, and the intensity reduction of the $(111)[1\bar{2}1]$ and $(111)[\bar{1}\bar{1}1]$ components during the grain size increase from ASTM 8.07 to ASTM 6.87 (figure 4). On the other hand, the ΔR was reduced throughout the grain growth process due to the reduced components, such as the Rotated Cube $(001)[\bar{1}\bar{1}0]$, of Theta fiber.

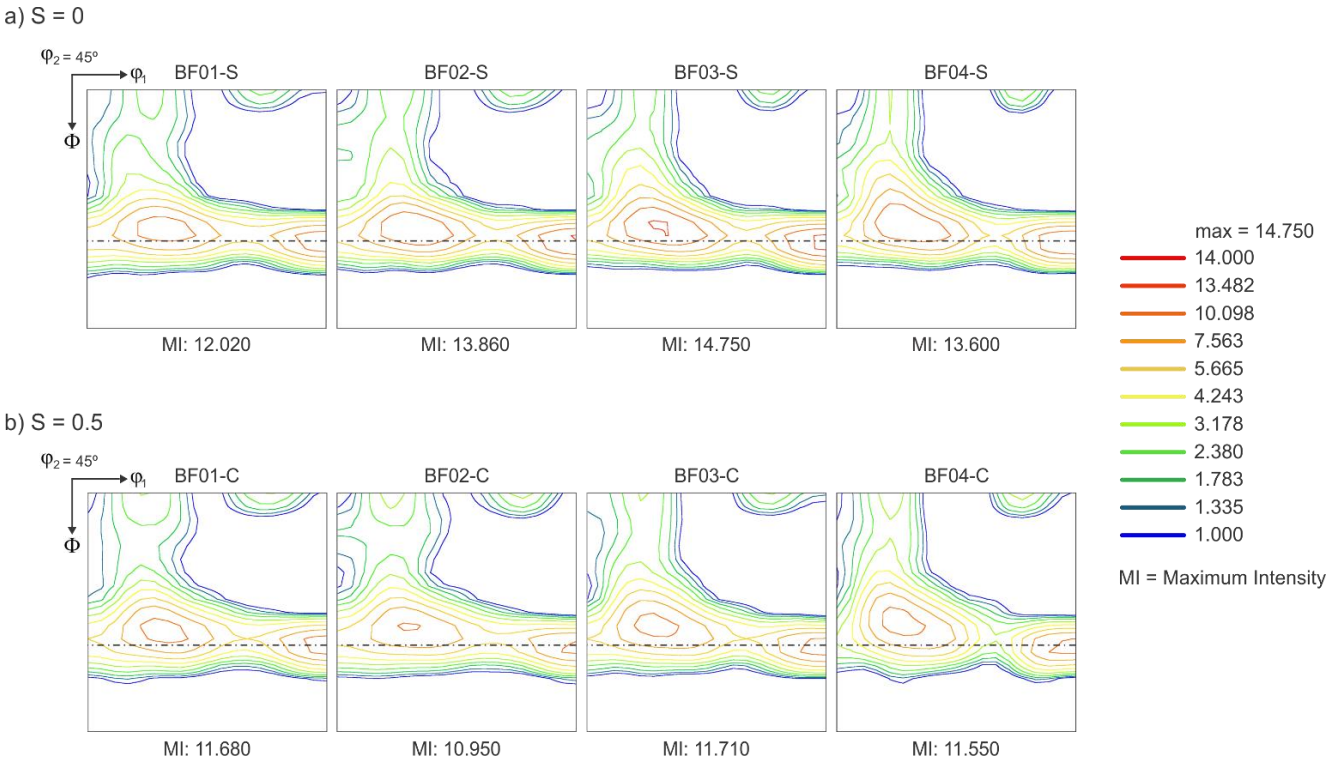

Figure 3. Recrystallization textures of the samples, where (a) $s = 0$ (BFXX-S) represents the surface layer and (b) $s = 0.5$ (BFXX-C) represents the center layer.

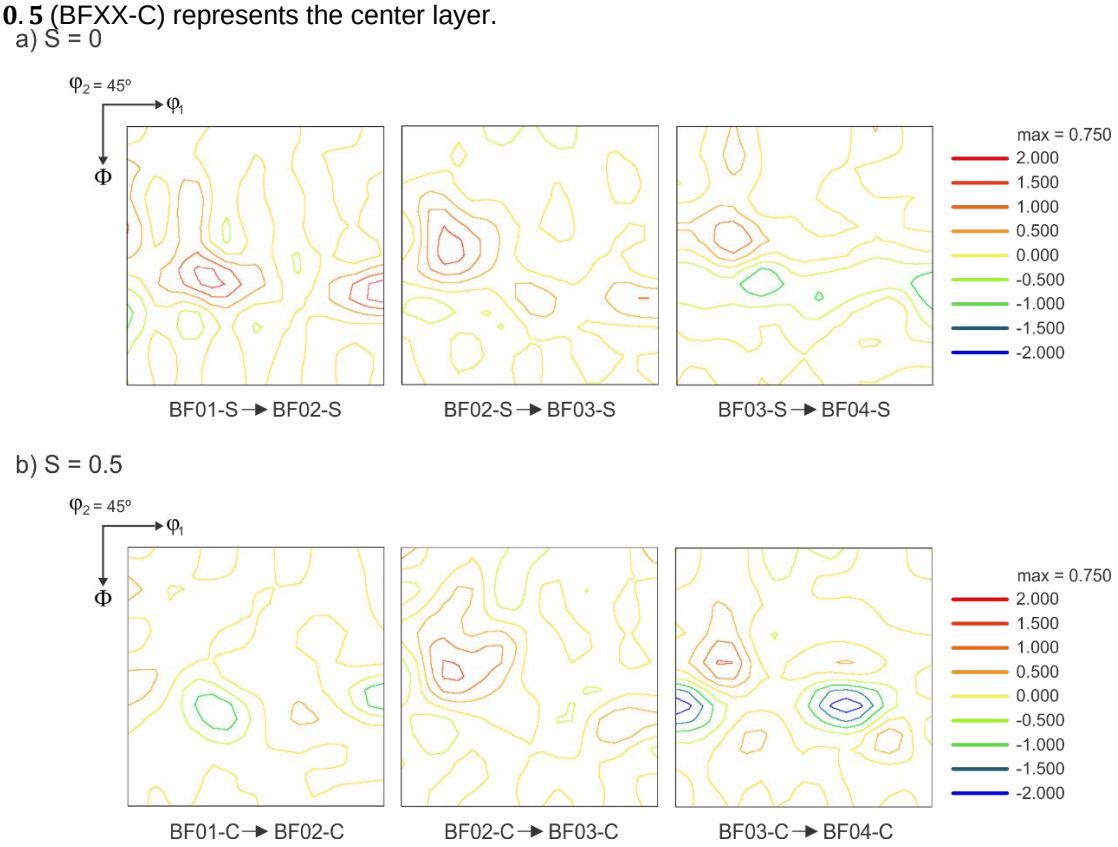

Figure 4. Texture changing shown by subtraction of ODFs samples in function of grain growth. where (a) $s = 0$ represents the surface layer and (b) $s = 0,5$ represents the center layer.

4 ADJUSTMENTS IN FINAL INDUSTRIAL HEAT TREATMENT PROCESS

The final heat treatment is responsible for promoting the recrystallization of the cold rolled coils. After this process, the coils are called BFs. Studies [3, 11, 12] show that increasing grain size in this process promotes the increase of r and reduction of ΔR, due to the increase of the gamma fiber and reduction of theta fiber [4,9]. Figures 5 and 6 show the correlation between the average grain size, Gamma/Theta ratio and average normal anisotropy (r) of 430Nb stainless steel coils with 0.6 mm thickness in different annealing conditions.

Grains with (111)//ND orientations grow faster than other crystallographic orientations during the recrystallization process [3]. For this reason, materials with higher grains sizes have greater formability. However, the increase in grain size increases the risk of the appearance Lüders bands after stamping process [3, 9].

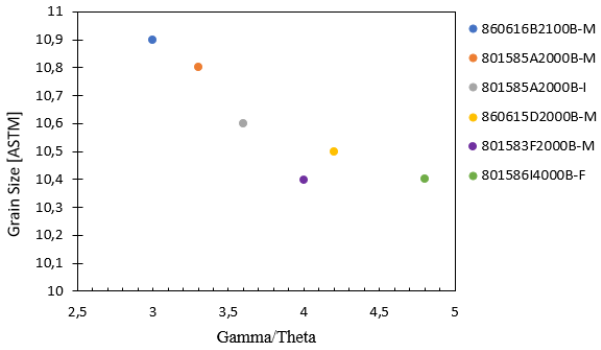

Figure 5. Correlation between average grain size and Gamma/Theta ratio of coils.

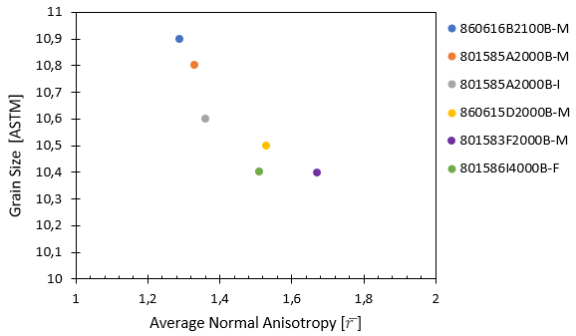

Figure 6. Correlation between average grain size and average normal anisotropy of coils.

Based on this information, the parameters of the final heat treatment were changed in order to promote the increase of the BFs grain size. The average speed process in the cold annealed and pickling line (CAPL#4) was reduced by 15% aiming to increase the materials exposure to heat. In addition, the furnace temperatures were increased in the last heating zones in order to increase the soaking temperature by 20°C.

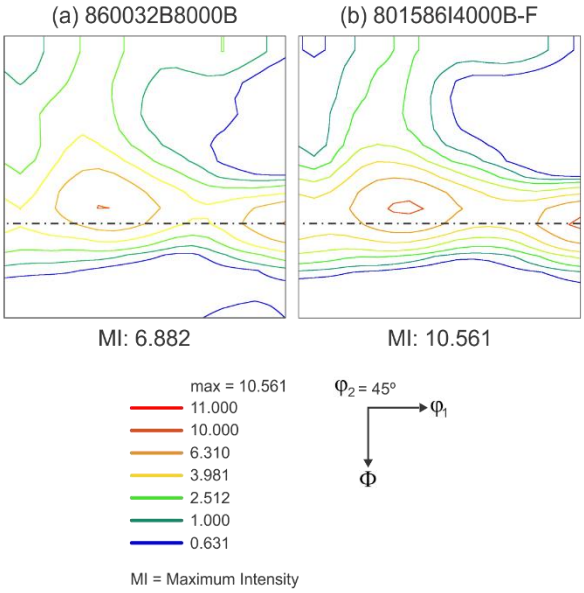

Figure 7. Coils ODFs, where (a) 860032B8000B and (b) 801586I4000B-F.

Figure 7 presents the texture comparison between two coils produced with different furnace parameters. ODF (a) shows the texture of a coil that was produced with 15% higher speed and a soaking temperature of 20°C lower than the coil (b).

The recrystallization texture of the coils got a maximum intensity in $(334)[4\bar{8}3]$ component. The other higher intensity was found at $(111)[\bar{1}\bar{1}2]$. The ODF shown in figure 7 (a) presents a texture with a less intense Gamma fiber, Goss $(110)[001]$ components and higher intensity Theta fiber, when compared to the ODF shown in figure 7 (b). Therefore, the texture of the coil shown in figure 7 (b) is more favorable for deep drawing applications.

5 CONCLUSIONS

As a conclusion, the following facts can be cited:

The normal anisotropy (r) was increased in all directions and the average planar anisotropy (ΔR) was decreased with increasing grain size until to ASTM 8.07 (optimum point). The increase in formability occurred due to increase the intensity Gamma fiber components, $(111)[1\bar{2}1]$ and $(111)[\bar{1}\bar{1}2]$, and reduction of the intensity of the Rotated Cube $(001)[\bar{1}\bar{1}0]$ and other Theta fiber components.

During the grain size increase from ASTM 8.07 to ASTM 6.87, displaced orientations of Gamma fiber close to the orientation $(334)[4\bar{8}3]$ were intensified. This change in texture reduced the gamma fiber and, consequently, reduced the material formability.

The adjustments made in the final continuous annealing process promoted the increase average grain size of the coils and, consequently, increase the Gamma fiber intensity and reduced the Theta fiber intensity. Therefore, the coils processed with higher soaking temperatures showed better deep drawability.

Acknowledgments

The authors gratefully acknowledge financial and technical support from

Aperam South America and Centro Universitário de Minas Gerais (Unileste).

REFERENCES

1 Oliveira TR; Alves HJ; Lopes RG; Guida RB, et al. Influência da textura e da microestrutura na estampabilidade dos aços inoxidáveis ferríticos 430 estabilizados ao nióbio, 2008, In: 63º Congresso da Associação Brasileira de Materiais.

2 Oliveira TR. Effet du niobium et du titane sur la déformation à chaud d'aciers inoxydables ferritiques stabilisés [tese de doutorado]. Saint-Étienne: Escole de Mines de Saint-Étienne, 2003.

3 Oliveira TR; Silva RC; Alcântara CM; Lopes RG; Ferreira JS; Arthuso EM; et al. Aço inoxidável ferrítico tipo ASTM 430 para estampagem profunda, com alto brilho e isento de estriamento, 2013, In: 68º Congresso annual da Associação Brasileira de Materiais.

4 Yazawa Y; Osaki Y; Kato Y; Furukimi O. Development of ferritic stainless steel sheets with excellent deep drawability by {111} recrystallization texture control. JSAE Review. 2003; 24(4): 483 - 488.

5 Lee KM; Engler O; Huh MY; Effect of texture components on the Lankford parameters in ferritic stainless steel sheets. ISIJ International. 2011; 53(3): 522-529.

6 American Society for Testing and Materials. ASTM E112-13: Standard Tests Methods for Determining Average Grain Size. West Conshohocken, 2013.

7 American Society for Testing and Materials. ASTM E8 / E8M-16ª: Standard Test Methods for Tension Testing of Metallic Materials. Wet Conshohocken, 2016.

8 Padilha, A; Siciliano, F. Encruamento, Rescristalização, Crescimento de Grão e Textura. 3. ed. São Paulo: Associação Brasileira de Materiais; 2005.

9 Jaskarin, M; Jarvenpaa, A; Karjalainen, P; The Effect of Heating Rate on Texture and Formability of Ti-Nb Stabilized Ferritic Stainless Steel. 2018. 786. 3 – 9.

10 Raabe, D; Lucke, K; Selective Particle Drag During Primary Recrystallization of Fe-Cr Alloys. 1992. 26. 19 – 24.

11 Tanure, L; Alcantara, M; Oliveira, T; Santos, D; Gonzalez, B. Microstructure, Texture and Microhardness Evolution during Annealing Heat Treatment and Mechanical Behavior of the Niobium-Stabilized Ferritic Stainless Steel ASTM 430 and Noibium-Titanium-Stabilized Ferritic Stainless Steel ASTM 439: a Comparative Study. Materials Research. 2017. 20(6): 1650 – 1657.

12 Abreu, H F; Bruno, A D; Tavares, S S; Santos, R P; Carvalho, S S. Effect of High Temperature Annealing on Texture and Microstructure on an AISI-444 Ferritic Stainless Steel. 2006. 57. 342 – 347.